Higher Order Hybrid FEM-MoM Technique for Analysis of Antennas and Scatterers

Milan M. Ilić, *Member, IEEE*, Miroslav Djordjević, *Member, IEEE*, Andjelija Ž. Ilić, *Member, IEEE*, and Branislav M. Notaroš, *Senior Member, IEEE*

***Abstract*—A novel higher order large-domain hybrid computational electromagnetic technique based on the finite element method (FEM) and method of moments (MoM) is proposed for three-dimensional analysis of antennas and scatterers in the frequency domain. The geometry of the structure is modeled using generalized curved parametric hexahedral and quadrilateral elements of arbitrary geometrical orders. The fields and currents on elements are modeled using curl- and divergence-conforming hierarchical polynomial vector basis functions of arbitrary approximation orders, and the Galerkin method is used for testing. The elements can be as large as about two wavelengths in each dimension. As multiple MoM objects are possible in a global exterior region, the MoM part provides much greater modeling versatility and potential for applications, especially in antenna problems, than just as a boundary-integral closure to the FEM part. The examples demonstrate excellent accuracy, convergence, efficiency, and versatility of the new FEM-MoM technique, and very effective large-domain meshes that consist of a very small number of large flat and curved FEM and MoM elements, with p-refined field and current distributions of high approximation orders. The reduction in the number of unknowns is by two orders of magnitude when compared to available data for low-order FEM-MoM modeling.**

***Index Terms*—Antennas, curved parametric elements, electromagnetic analysis, finite element method (FEM), higher order modeling, hybrid methods, method of moments (MoM), numerical techniques, polynomial basis functions, scattering.**

I. Introduction

HYBRID FINITE element-boundary integral (FE-BI) techniques are extremely powerful and versatile general numerical tools for electromagnetic simulations in radiation and scattering applications [1]–[5]. They introduce exact BI terminations to numerically truncate and close the computational domain in modeling of unbounded problems (antennas and scatterers) based on the finite element method (FEM). Basically, the techniques divide the problem into an interior and exterior region. The electromagnetic field in the interior region, usually containing inhomogeneous materials, is modeled employing an FE differential-equation formulation and the field in the exterior region, filled with a homogeneous medium (most frequently, free space), is represented by some sort of BI equations. The fields are then coupled across the FE-BI interface by means of the appropriate boundary conditions. The coupled system of differential and integral equations is solved using various FE and BI numerical discretizations. Since the latter computational methodologies correspond to solutions of surface integral equations (SIEs) based on the method of moments (MoM), the hybrid methods are also referred to as FEM-MoM techniques.

A tremendous amount of effort has been invested in the research of FE-BI techniques in the past two decades. This led to many improvements of the original ideas and a number of novel techniques have been developed. A simple and effective FEM-MoM hybridization concept is given in [6] and [7], followed by a review of contemporary hybrid techniques in [8] and study of a variety of FE-BI formulations for three-dimensional (3-D) electromagnetic scattering by inhomogeneous objects and development of a novel technique immune to the problem of interior resonances, which also employs the multilevel fast multipole algorithm (MLFMA) to accelerate the BI portion of the technique [9]. A hybrid symmetric FEM-MoM formulation, which leads to a symmetric FE-BI matrix, has been derived in [10], and generalized to an efficient 3-D symmetric hybrid technique in [11]. Recent works also include a nonstandard BI approach to FEM domain truncation based on an adaptive numerical absorbing boundary condition (ABC) [12], efficient preconditioning using a FE-ABC matrix as a preconditioner for the FE-BI method [13], evaluation of performances of a variety of symmetric hybrid formulations [14], further investigation of problems of interior resonances [14], [15], FE-BI hybridization in the time domain [16], and FE-BI analysis and design of complex antennas [5], [17], [18].

However, in terms of the particulars of the numerical discretizations, most FEM-MoM (or FE-BI) tools are low-order (also referred to as small-domain or subdomain) techniques—the radiation or scattering structure under consideration is modeled by volume and surface geometrical elements that are electrically very small, on the order of $\lambda/10$ in each dimension, λ being the wavelength in the medium, and the fields and currents within the elements are approximated by low-order (zeroth-order and first-order) basis functions.

Manuscript received August 23, 2008; revised December 28, 2008. Current version published May 06, 2009. This work was supported by the National Science Foundation under grants ECCS-0647380 and ECCS-0650719, and by the Serbian Ministry of Science and Technological Development under Grant ET-11021.

M. M. Ilić is with School of Electrical Engineering, University of Belgrade, 11120 Belgrade, Serbia and also with the Department of Electrical and Computer Engineering, Colorado State University, Fort Collins, CO 80523-1373 USA (e-mail: milanilic@etf.rs).

M. Djordjević is with ICT College, 11000 Belgrade, Serbia Serbia and also with the Department of Electrical and Computer Engineering, Colorado State University, Fort Collins, CO 80523-1373 USA (e-mail: miroslav@ieee.org).

A. Ž. Ilić is with the Laboratory of Physics 010, Vinca Institute of Nuclear Sciences, 11001 Belgrade, Serbia and also with the School of Electrical Engineering, University of Belgrade, 11120 Belgrade, Serbia (e-mail: andjelijailic@ieee.org).

B. M. Notaroš is with the Department of Electrical and Computer Engineering, Colorado State University, Fort Collins, CO 80523-1373 USA (e-mail: notaros@colostate.edu).

Digital Object Identifier 10.1109/TAP.2009.2016725

This results in a very large number of unknowns (unknown field/current distribution coefficients) needed to obtain results of satisfactory accuracy, with all the associated problems and enormous requirements in computational resources. In addition, commonly used geometrical elements are solids with planar sides and flat patches, and thus they do not provide enough flexibility and efficiency in modeling of structures with pronounced curvature. An alternative is the higher order (also known as the large-domain or entire-domain) computational approach [19], which utilizes higher order field/current basis functions defined on large (e.g., on the order of λ in each dimension) curvilinear geometrical elements.

Only recently higher order FEM-MoM techniques have been proposed, developed, and employed in analysis of high-frequency unbounded electromagnetic structures [5], [12]–[14], [16], [20]–[22], with an objective to significantly reduce the number of unknowns and computational resources for a given (high) accuracy when compared to low-order solutions. However, none of the proposed techniques exploits the full potential of the higher order FE and BI modeling and all of the actually reported results are limited to the utilization of basis functions of the second or third order. In addition, these techniques still implement small finite and boundary elements for field/current modeling, and the higher order meshes reported actually represent small-domain solutions to the electromagnetic problems considered. Note also that some of the tools are restricted to 2.5-D problems, that is, body of revolution (BOR) geometries [22], and some to higher order implementations only in the FEM region of the problem [20]–[22], which is often dictated by the specific intended application of the tool. Finally, it appears that all of the existing higher order FE-BI techniques are presented and applied as scattering codes; all results are for electromagnetic scatterers, and no antenna examples seem to be reported.

This paper proposes a novel higher order large-domain Galerkin-type hybrid FEM-MoM technique for 3-D electromagnetic analysis of arbitrary antennas and scatterers in the frequency domain, based on approximations of arbitrarily high orders for both geometrical modeling and field/current modeling, in both FEM and MoM regions. The solution in the interior region of the problem is obtained by a higher order FEM for discretizing the curl-curl electric-field vector wave equation [23], [24]. The solution in the exterior region is based on a higher order MoM for discretizing the set of coupled electric/magnetic field integral equations (EFIE/MFIE) with electric and magnetic surface currents as unknowns [25]. The two methods are coupled together at the boundary of the interior (FEM) region via boundary conditions. The FEM-MoM interface can be moved some distance away from the actual objects within the FEM domain (e.g., when the objects are metallic), or it can coincide with the object boundary surface (e.g., for dielectric objects). To the best of our knowledge, this is the first truly high-order hybrid computational electromagnetic technique combining the solutions to volume partial differential equations and surface integral equations. It combines the features of the previously proposed FEM and MoM techniques [23]–[25] in a unified numerical framework and with a full higher order computational effectiveness taking advantage of curl- and divergence-conforming hierarchical polynomial vector approximations of volumetric fields and surface currents within the electrically large Lagrange-type parametric volume and surface finite and boundary elements (large domains). The new method enables using as large as about $2\lambda \times 2\lambda \times 2\lambda$ curved FEM hexahedra and $2\lambda \times 2\lambda$ curved MoM quadrilaterals as building blocks for modeling of the antenna or scatterer (which is 20 times the traditional low-order modeling discretization limit). However, higher order solutions should be applied and will be truly beneficial only for smooth regions, where large elements are possible. More precisely, because the implemented basis functions are hierarchical, element orders in the model can also be low, so that the low-order modeling approach is actually included in the higher order modeling and both large and small elements can be combined together in the same model, but clearly the proposed method is most suitable for problems where the most of the structure can be tessellated using large higher order curved elements. In terms of excitation and operation of the structure, the technique is equally suitable for antenna and scattering applications. Finally, the proposed technique can incorporate multiple MoM objects and FEM sub-regions in a global generally unbounded MoM domain, and thus is not strictly dependent on the standard FE-BI scheme. This is quite important, as the MoM part of the technique provides much greater modeling versatility and potential for applications than just as a BI closure to the FEM part.

Section II of this paper presents the theoretical background and numerical components of the new higher order hybrid FEM-MoM technique. Along with some necessary derivations and facts pertaining to the FEM representation of the interior region and MoM treatment of the exterior problem, the emphasis is placed on the actual hybridization of the two methodologies and numerical techniques. In Section III, the technique is validated and its accuracy, convergence, and efficiency evaluated and discussed in several characteristic examples.

II. Theory and Implementation

Consider an electromagnetic system consisting of arbitrarily shaped metallic and dielectric bodies. Let the system be excited by a time-harmonic electromagnetic field of complex field intensities $\mathbf{E}^{\mathrm{inc}}$ and $\mathbf{H}^{\mathrm{inc}}$, and angular frequency ω. This field may be a combination of incident plane waves (for a scattering structure) or the impressed field of one or more lumped generators (for an antenna structure). As the first step of the analysis, we decompose the system into two parts: a MoM (exterior) region and a FEM (interior) region, and denote them as regions a and b, respectively, as shown in Fig. 1. In general, multiple MoM and multiple FEM objects can exist in an overall MoM environment. In this arrangement, for example, homogeneous dielectric domains can be modeled as parts of the FEM region or as MoM objects (via surface equivalence principle). Metallic objects (e.g., metallic wires or plates) in the external medium (most frequently, air), on the other hand, can be modeled as MoM objects (using surface electric currents) or they can be enclosed in a virtual dielectric (air) domain and treated as a FEM sub-region.

The total electric and magnetic field intensity vectors in region a, $\mathbf{E}^a$ and $\mathbf{H}^a$, are expressed in terms of the equivalent surface electric current, of density $\mathbf{J}_{\mathrm{S}}$, and equivalent surface magnetic current, of density $\mathbf{M}_{\mathrm{S}}$, that are placed on the outer

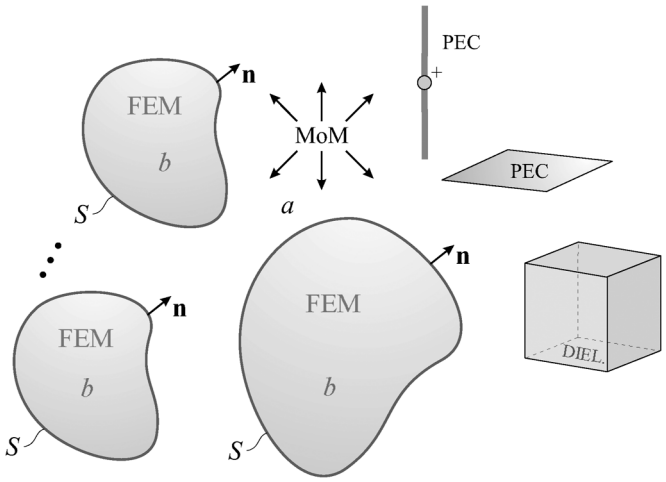

Fig. 1. Decomposition of an electromagnetic structure into a MoM (exterior) and a FEM (interior) region, denoted as regions a and b, respectively.

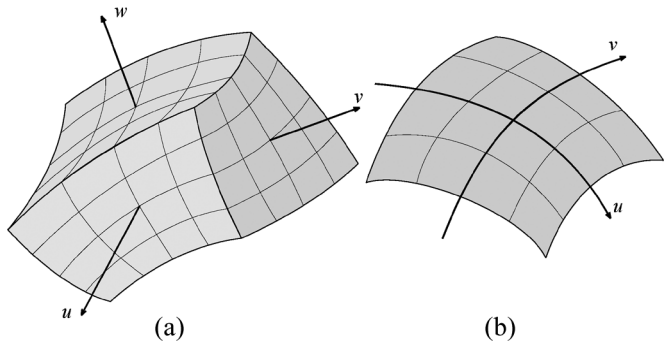

Fig. 2. Lagrange-type curved parametric elements for geometrical modeling in the higher order FEM-MoM method: (a) generalized hexahedron and (b) generalized quadrilateral.

boundaries (surface S) of all objects in region b, and the incident or impressed field vectors as follows:

$$\begin{aligned}\mathbf{E}^a &= \mathbf{E}_{\mathrm{J}}(\mathbf{J}_{\mathrm{S}}) + \mathbf{E}_{\mathrm{M}}(\mathbf{M}_{\mathrm{S}}) + \mathbf{E}^{\mathrm{inc}} \\ \mathbf{H}^a &= \mathbf{H}_{\mathrm{J}}(\mathbf{J}_{\mathrm{S}}) + \mathbf{H}_{\mathrm{M}}(\mathbf{M}_{\mathrm{S}}) + \mathbf{H}^{\mathrm{inc}}\end{aligned} \tag{1}$$

where $\mathbf{E}_{\mathrm{J}}$ and $\mathbf{H}_{\mathrm{J}}$ stand for the scattered electric and magnetic field vectors due to current $\mathbf{J}_{\mathrm{S}}$, while $\mathbf{E}_{\mathrm{M}}$ and $\mathbf{H}_{\mathrm{M}}$ are the scattered fields due to $\mathbf{M}_{\mathrm{S}}$. These fields are computed as

$$\begin{aligned}\mathbf{E}_{\mathrm{J}}(\mathbf{J}_{\mathrm{S}}) &= -\mathrm{j}\omega\mathbf{A} - \nabla\Phi, \quad \mathbf{E}_{\mathrm{M}}(\mathbf{M}_{\mathrm{S}}) = -\frac{1}{\varepsilon}\nabla\times\mathbf{F} \\ \mathbf{H}_{\mathrm{M}}(\mathbf{M}_{\mathrm{S}}) &= -\mathrm{j}\omega\mathbf{F} - \nabla U, \quad \mathbf{H}_{\mathrm{J}}(\mathbf{J}_{\mathrm{S}}) = \frac{1}{\mu}\nabla\times\mathbf{A}\end{aligned} \tag{2}$$

with ε and μ being the complex permittivity and permeability of the medium (exterior to S). The electromagnetic potentials are given by

$$\begin{aligned}\mathbf{A} &= \mu\int_S \mathbf{J}_{\mathrm{S}} g\,\mathrm{d}S, \quad \mathbf{F} = \varepsilon\int_S \mathbf{M}_{\mathrm{S}} g\,\mathrm{d}S \\ \Phi &= \frac{\mathrm{j}}{\omega\varepsilon}\int_S \nabla_{\mathrm{S}}\cdot\mathbf{J}_{\mathrm{S}} g\,\mathrm{d}S, \quad U = \frac{\mathrm{j}}{\omega\mu}\int_S \nabla_{\mathrm{S}}\cdot\mathbf{M}_{\mathrm{S}} g\,\mathrm{d}S\end{aligned} \tag{3}$$

where g is Green's function for the unbounded homogeneous medium of parameters ε and μ

$$g = \frac{\mathrm{e}^{-\gamma R}}{4\pi R}, \quad \gamma = \mathrm{j}\omega\sqrt{\varepsilon\mu} \tag{4}$$

γ being the propagation coefficient in the medium and R the distance of the field point from the source point.

The fields $\mathbf{E}^a$ and $\mathbf{H}^a$ are coupled to the corresponding field vectors in region b, $\mathbf{E}^b$ and $\mathbf{H}^b$, through boundary conditions for the tangential field components on the surface S

$$(\mathbf{E}^a)_{\tan} = (\mathbf{E}^b)_{\tan} \tag{5}$$

$$(\mathbf{H}^a)_{\tan} = (\mathbf{H}^b)_{\tan} = \mathbf{J}_{\mathrm{S}}\times\mathbf{n} \tag{6}$$

where $\mathbf{n}$ is the outward unit normal on S. Combined with (1), the conditions yield

$$-[\mathbf{E}_{\mathrm{J}}(\mathbf{J}_{\mathrm{S}})]_{\tan} - [\mathbf{E}_{\mathrm{M}}(\mathbf{M}_{\mathrm{S}})]_{\tan} + (\mathbf{E}^b)_{\tan} = (\mathbf{E}^{\mathrm{inc}})_{\tan} \tag{7}$$

$$-[\mathbf{H}_{\mathrm{J}}(\mathbf{J}_{\mathrm{S}})]_{\tan} - [\mathbf{H}_{\mathrm{M}}(\mathbf{M}_{\mathrm{S}})]_{\tan} + \mathbf{J}_{\mathrm{S}}\times\mathbf{n} = (\mathbf{H}^{\mathrm{inc}})_{\tan} \tag{8}$$

thus providing the computational interface between the MoM and FEM regions, with currents $\mathbf{J}_{\mathrm{S}}$ and $\mathbf{M}_{\mathrm{S}}$ over S and field $\mathbf{E}^b$ throughout region b (FEM region) as unknowns. In the FEM-MoM discretization procedure, these quantities are represented as

$$\mathbf{J}_{\mathrm{S}} = \sum_{j=1}^{N_{\mathrm{MoM}}} \alpha_j \mathbf{j}_{\mathrm{S}_j}, \quad \mathbf{M}_{\mathrm{S}} = \sum_{j=1}^{N_{\mathrm{MoM}}} \beta_j \mathbf{j}_{\mathrm{S}_j} \tag{9}$$

$$\mathbf{E}^b = \sum_{l=1}^{N_{\mathrm{FEM}}} \gamma_l \mathbf{e}_l \tag{10}$$

where $\mathbf{j}_{\mathrm{S}_j}$ are the adopted MoM basis functions, with unknown current-distribution coefficients α_j and β_j, whose total number on the FEM-MoM interface is $2N_{\mathrm{MoM}}$, while $\mathbf{e}_l$ are FEM basis functions, with a total of N_{FEM} unknown field-distribution coefficients γ_l. In specific, functions $\mathbf{e}_l$ are higher order curl-conforming hierarchical polynomial vector bases defined on Lagrange-type generalized curved parametric hexahedra of arbitrary geometrical orders in Fig. 2(a) [23]. On the other side, functions $\mathbf{j}_{\mathrm{S}_j}$ are the 2-D and divergence-conforming version of FEM bases on boundary elements in the form of generalized quadrilaterals in Fig. 2(b) [25], which are the 2-D version of hexahedral elements. With such exact compatibility of volume and surface geometrical elements, and field and current approximations, the hybridization of the two methods is performed in a true higher order fashion, with respect to both geometrical modeling and field/current modeling, in both FEM and MoM regions.

For MoM computations in region a, the tangential-field boundary conditions on the boundary surface between any two adjacent homogeneous dielectric domains (domains 1 and 2) can be written as [25]

$$\begin{aligned}&[\mathbf{E}(\mathbf{J}_{\mathrm{S}}, \mathbf{M}_{\mathrm{S}}, \varepsilon_1, \mu_1)]_{\tan} + (\mathbf{E}^{\mathrm{inc}})_{\tan} \\ &\quad = [\mathbf{E}(-\mathbf{J}_{\mathrm{S}}, -\mathbf{M}_{\mathrm{S}}, \varepsilon_2, \mu_2)]_{\tan}\end{aligned} \tag{11}$$

$$\begin{aligned}&[\mathbf{H}(\mathbf{J}_{\mathrm{S}}, \mathbf{M}_{\mathrm{S}}, \varepsilon_1, \mu_1)]_{\tan} + (\mathbf{H}^{\mathrm{inc}})_{\tan} \\ &\quad = [\mathbf{H}(-\mathbf{J}_{\mathrm{S}}, -\mathbf{M}_{\mathrm{S}}, \varepsilon_2, \mu_2)]_{\tan}\end{aligned} \tag{12}$$

where we assume that the incident (impressed) fields are present only in domain 1. On the perfectly conducting bodies, only condition (11) applies, which, for metallic surfaces in domain 1, reduces to

$$[\mathbf{E}(\mathbf{J}_{\mathrm{S}}, \mathbf{M}_{\mathrm{S}}, \varepsilon_1, \mu_1)]_{\tan} + (\mathbf{E}^{\mathrm{inc}})_{\tan} = 0. \tag{13}$$

The scattered fields, due to currents $\mathbf{J}_{\mathrm{S}}$ and $\mathbf{M}_{\mathrm{S}}$, are expressed as in (2)–(4), using the respective material parameters for domain 1 or 2, and the currents are, in turn, approximated by means of higher order basis functions $\mathbf{j}_{\mathrm{S}_j}$ as in (9), which, of course, adds to the total count of unknown current-distribution coefficients (α_j and β_j) in the MoM region, for the overall FEM-MoM computational model.

To solve for the coefficients γ_l in the FEM region of the model, the field expansion (10) is substituted in the curl-curl electric-field vector wave equation [23]

$$\nabla \times \mu_{\mathrm{r}}^{-1} \nabla \times \mathbf{E} - k_0^2 \varepsilon_{\mathrm{r}} \mathbf{E} = 0 \tag{14}$$

with ε_{r} and μ_{r} standing here for the complex relative permittivity and permeability of the inhomogeneous (possibly lossy) medium of region b, and $k_0 = \omega\sqrt{\varepsilon_0 \mu_0}$ is the free-space wave number. A standard Galerkin weak-form discretization of (14) yields

$$\int_V \mu_{\mathrm{r}}^{-1} (\nabla \times \mathbf{e}_k) \cdot (\nabla \times \mathbf{E}) \mathrm{d}V - k_0^2 \int_V \varepsilon_{\mathrm{r}} \mathbf{e}_k \cdot \mathbf{E} \mathrm{d}V = \mathrm{j} k_0 Z_0 \oint_S \mathbf{e}_k \cdot \mathbf{n} \times \mathbf{H} \mathrm{d}S \tag{15}$$

where V is the volume of region b (bounded by S), $\mathbf{e}_k$ are testing functions [the same as basis functions in (10)], and Z_0 is the free-space impedance. The matrix form of the FEM equation is obtained by substituting the expansion (10) into (15), on its left-hand side, and (6) and the first expansion in (9) on the right-hand side, so we have

$$[\mathrm{FEM}_{kl}]\{\gamma_l\} = [C_{kj}]\{\alpha_j\} \tag{16}$$

with $\{\gamma\}$ and $\{\alpha\}$ being the unknown vectors of FEM field and MoM electric-current distribution coefficients, in (10) and (9), respectively. The FEM matrix can be written as

$$[\mathrm{FEM}] = [A] - k_0^2 [B] \tag{17}$$

where the elements of matrices $[A]$ and $[B]$ are

$$[A_{kl}] = \int_V \mu_{\mathrm{r}}^{-1} (\nabla \times \mathbf{e}_k) \cdot (\nabla \times \mathbf{e}_l) \mathrm{d}V$$

and

$$[B_{kl}] = \int_V \varepsilon_{\mathrm{r}} \mathbf{e}_k \cdot \mathbf{e}_l \mathrm{d}V. \tag{18}$$

The matrix $[C]$ in (16) is given by

$$[C_{kj}] = \mathrm{j} k_0 Z_0 \left[\langle \mathbf{e}_k, \mathbf{j}_{\mathrm{S}_j} \rangle \right] \tag{19}$$

and the inner product of the FEM and MoM basis functions is

$$\langle \mathbf{e}_k, \mathbf{j}_{\mathrm{S}_j} \rangle = \oint_S \mathbf{e}_k \cdot \mathbf{j}_{\mathrm{S}_j} \mathrm{d}S. \tag{20}$$

On the other side, Galerkin discretization of (7) and (8), with testing and basis functions in (9), yields the SIE matrix equation over the FEM-MoM interface (surface S)

$$\begin{bmatrix} -\langle \mathbf{j}_{\mathrm{S}_i}, \mathbf{E}_{\mathrm{J}} (\mathbf{j}_{\mathrm{S}_j}) \rangle + \langle \mathbf{j}_{\mathrm{S}_i}, \mathbf{E}^b (\mathbf{j}_{\mathrm{S}_j}) \rangle & -\langle \mathbf{j}_{\mathrm{S}_i}, \mathbf{E}_{\mathrm{M}} (\mathbf{j}_{\mathrm{S}_j}) \rangle \\ -\langle \mathbf{j}_{\mathrm{S}_i}, \mathbf{H}_{\mathrm{J}} (\mathbf{j}_{\mathrm{S}_j}) \rangle + \langle \mathbf{j}_{\mathrm{S}_i}, \mathbf{j}_{\mathrm{S}_j} \times \mathbf{n} \rangle & -\langle \mathbf{j}_{\mathrm{S}_i}, \mathbf{H}_{\mathrm{M}} (\mathbf{j}_{\mathrm{S}_j}) \rangle \end{bmatrix} \times \begin{bmatrix} \{\alpha_j\} \\ \{\beta_j\} \end{bmatrix} = \begin{bmatrix} \langle \mathbf{j}_{\mathrm{S}_i}, \mathbf{E}^{\mathrm{inc}} \rangle \\ \langle \mathbf{j}_{\mathrm{S}_i}, \mathbf{H}^{\mathrm{inc}} \rangle \end{bmatrix} \tag{21}$$

which can be conveniently represented as

$$\begin{bmatrix} [-Z_{ij}^{ee} + \langle \mathbf{j}_{\mathrm{S}_i}, \mathbf{E}^b (\mathbf{j}_{\mathrm{S}_j}) \rangle] & [-Z_{ij}^{em}] \\ [-Z_{ij}^{me} + \langle \mathbf{j}_{\mathrm{S}_i} \times \mathbf{j}_{\mathrm{S}_j}, \mathbf{n}) \rangle] & [-Z_{ij}^{mm}] \end{bmatrix} \begin{bmatrix} \{\alpha_j\} \\ \{\beta_j\} \end{bmatrix} = \begin{bmatrix} \{v^e\}^{\mathrm{inc}} \\ \{v^m\}^{\mathrm{inc}} \end{bmatrix}. \tag{22}$$

All the terms in (22) can be readily evaluated except $\mathbf{E}^b(\mathbf{j}_{\mathrm{S}_j})$, for which we solve from (10) and (16) as follows:

$$\mathbf{E}^b \left(\mathbf{j}_{\mathrm{S}_{\hat{j}}} \right) = \sum_{l=1}^{N_{\mathrm{FEM}}} \gamma_l^{\hat{j}} \mathbf{e}_l = \left\{ \gamma_l^{\hat{j}} \right\}^{\mathrm{T}} \{\mathbf{e}_l\} \tag{23}$$

$$\left\{ \gamma_l^{\hat{j}} \right\} = [\mathrm{FEM}_{kl}]^{-1} \{C_{k\hat{j}}\} \tag{24}$$

where $\{C_{k\hat{j}}\}$ (with a fixed $j = \hat{j}$) stands for the $\hat{j}$th column of $[C_{kj}]$, and (23) and (24) are computed for all values of $\hat{j}$ from 1 to N_{MoM}.

Higher order FEM matrices are much smaller than their low order counterparts (the reduction of the number of unknowns is often measured by orders of magnitude, for the same or better accuracy) [23], [24], and are thus factored efficiently using sparse storage algorithms and direct sparse factorization techniques. In addition, [FEM] in (24) needs to be factored only once, after which coefficients in (24) and fields in (23) can be calculated one by one, using a fast back-substitution procedure. Note also that the FEM matrix elements in (17) depend on frequency only through k_0^2, provided that μ_{r} and ε_{r} are frequency independent (dispersionless media), which allows for the elements of the matrix to be calculated only once, for the entire frequency range of interest, and stored separately as matrices $[A]$ and $[B]$, from which [FEM] can be reconstructed, according to (17), for any given frequency. Note finally that alternative higher order hierarchical basis functions with improved orthogonality and conditioning properties constructed from Legendre polynomials [26] may be implemented in the technique as well.

Once all $\mathbf{E}^b(\mathbf{j}_{\mathrm{S}_j})$ terms are computed, the MoM matrix in (22) can be completed and the system solved for the unknown current distribution coefficients $\{\alpha_j\}$ and $\{\beta_j\}$, that is, by way of expansions (9), for the MoM surface currents $\mathbf{J}_{\mathrm{S}}$ and $\mathbf{M}_{\mathrm{S}}$ on S. Exterior fields (in the MoM region) can then be obtained using (2)–(4). Finally, the FEM field coefficients $\{\gamma_l\}$ can be found from (16)

$$\{\gamma_l\} = [\mathrm{FEM}_{kl}]^{-1} [C_{kj}] \{\alpha_j\} \tag{25}$$

and the interior electric field (within the FEM region) can be evaluated by means of the expansion (10).

On the FEM-MoM interface in a model, field expansion orders in a FEM hexahedron and current expansion orders on the attached MoM quadrilaterals are adopted based on the largest electrical length of the element in the specific direction, with the same or close values of the two sets of associated orders,

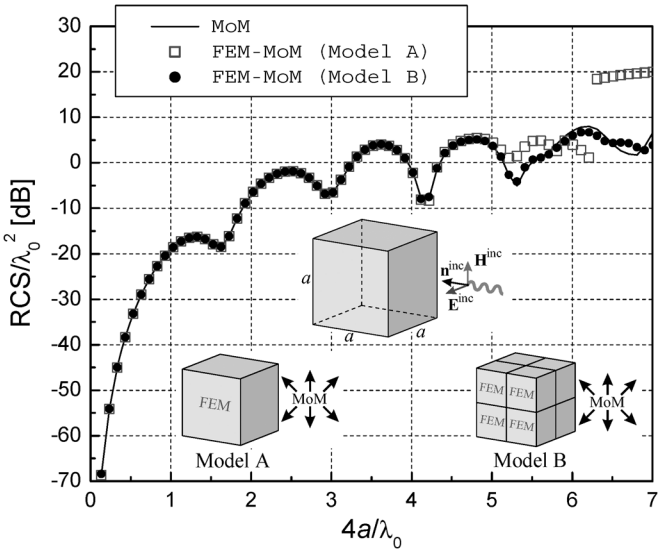

Fig. 3. Normalized monostatic radar cross section (RCS) of a dielectric ($\varepsilon_r = 2.25$) cube (λ_0 is the free-space wavelength): comparison of solutions obtained by two higher order FEM-MoM models (A and B) with the reference pure MoM solution.

for FEM and MoM computation. Numerical experiments have shown that optimal numbers of degrees of freedom for the desired accuracy are most often obtained when the difference between the two corresponding orders is (positive or negative) one. This can be attributed to the fact that dominant inner products in (20) are normally those between FEM and MoM basis functions in the same direction, whose maximal orders are offset by one in the mixed-order arrangement for curl-conforming functions [23] with respect to that for divergence-conforming functions [25].

III. Results and Discussion

All numerical results by the proposed higher order FEM-MoM technique are obtained using an IBM Thinkpad T60p notebook computer with Intel T7200 CPU running at 2.0 GHz under Microsoft Windows XP operating system.

As the first example, consider a lossless cubical dielectric scatterer of side length a, shown in the top inset of Fig. 3. Relative permittivity of the dielectric is $\varepsilon_r = 2.25$ (polyethylene). Fig. 3 presents the monostatic radar cross section (RCS) of the cube, normalized to λ_0^2, as a function of $4a/\lambda_0$, λ_0 being the free-space wavelength. The results obtained by two hybrid FEM-MoM higher order solutions, with (A) one FEM hexahedron and 6 MoM quadrilaterals and (B) 8 FEM hexahedra and 24 MoM quadrilaterals, are compared with the results obtained by the MoM [25] alone, as a reference solution. The FEM-MoM interface, S, is placed exactly on the cube surface in both hybrid models. Note that the FEM region in model A is literally an entire-domain FEM model (an entire computational domain is represented by a single finite element). Note also that the other higher order FEM-MoM solution is aimed to illustrate the model behavior when the number of elements is increased, which corresponds to an h-refinement of the model. In both models, sketched in the bottom insets of the figure, all elements are of the first geometrical order. In model A, the field expansion orders are 7 (in all directions) for the FEM hexahedron and current expansion orders are 6 for MoM quadrilaterals, while these orders are 5

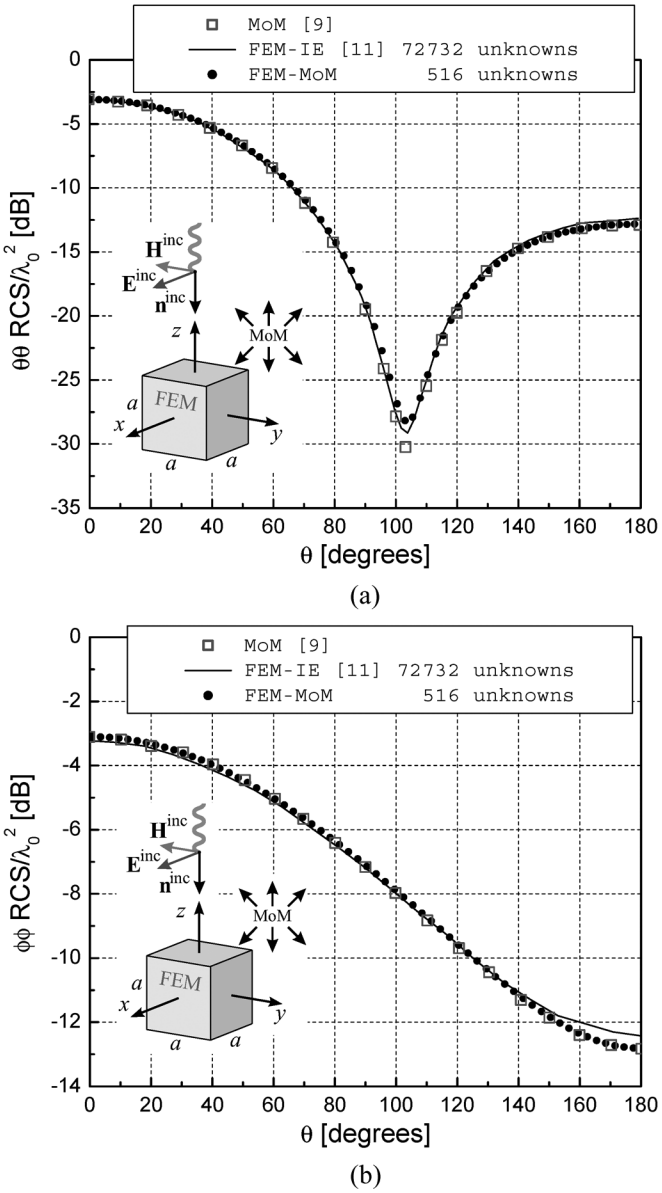

Fig. 4. Normalized bistatic radar cross section of a dielectric cube ($\varepsilon_r = 4$, $a = 0.3\lambda_0$) in xz-plane (a) and yz-plane (b): comparison of an entire-domain higher order FEM-MoM solution (model A in Fig. 3) and MoM [9] and low-order FEM-IE [11] solutions.

and 4, respectively, in model B. These arrangements yield a total of 1344 FEM and 864 MoM unknowns for model A and 3630 FEM and 1536 MoM unknowns for model B. It can be observed in the figure that the higher order hybrid solution accurately matches the reference MoM solution, and that it quickly converges when the structure is h-refined and the number of unknowns increased. Note that the entire-domain mesh (model A), which is the coarsest model possible, with the minimum number of elements, performs well up to the frequency at which $4a/\lambda_0 = 5$.

Next, we consider a dielectric cube with $\varepsilon_r = 4$ at the frequency where $a = 0.3\lambda_0$, and show in Fig. 4 the normalized bistatic RCS of the cube in two characteristic planes, for the direction of propagation and polarization of the incident plane wave indicated in the inset. The results of the higher order FEM-MoM method with the simplest (entire-domain) model (single cubical FEM element and 6 square MoM elements)

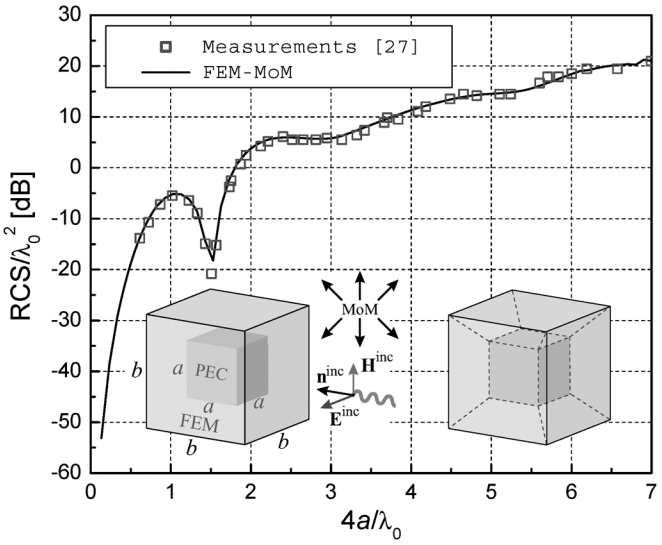

Fig. 5. Normalized monostatic radar cross section of a metallic cube: comparison of a higher order FEM-MoM solution using 6 FEM and 6 MoM elements (model includes an air box of side length $b = 1.04a$ around the cube) with experimental results [27].

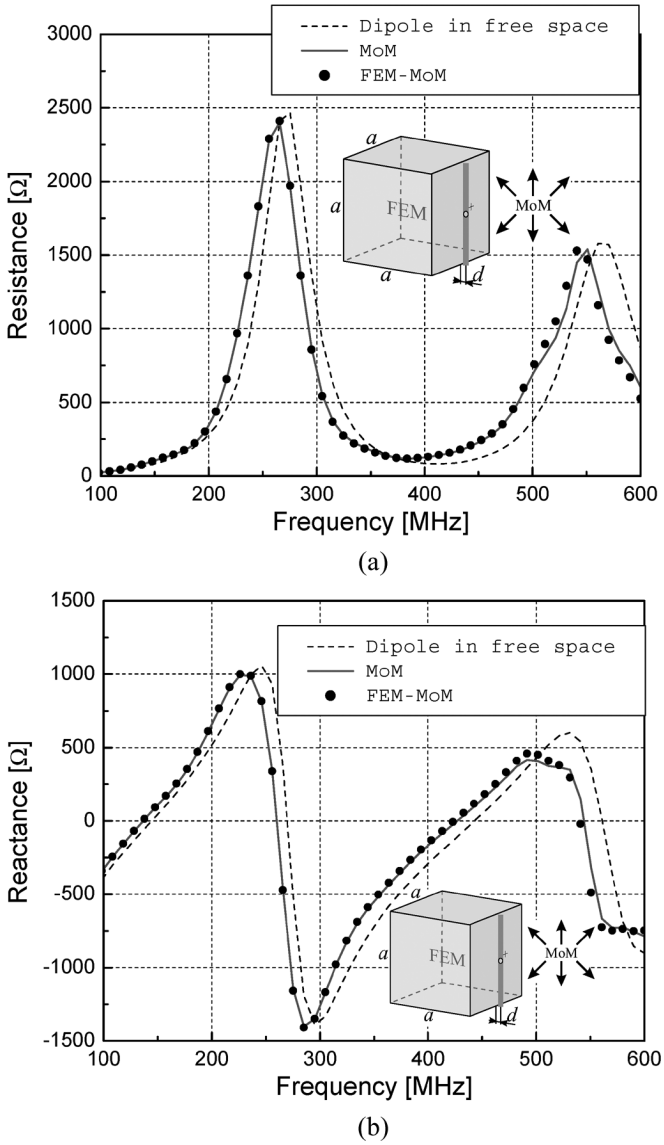

Fig. 6. Input resistance (a) and reactance (b) of a wire dipole antenna in the vicinity of a dielectric cube ($a = 1$ m, $d = 1$ cm, $\varepsilon_r = 2$): comparison of a higher order FEM-MoM solution (based on the model B in Fig. 3) and reference pure MoM results; Impedance of the dipole in free space is also shown.

are compared with the results obtained by the MoM [9] and low-order symmetric FEM-IE [11]. The orders of the polynomial field and current approximations in the FEM-MoM model are 4 and 3, respectively, resulting in as few as 300 FEM and 216 MoM unknowns. The required memory is 8.4 MB. The computation times for filling and solving the matrices are 2.9 s and 0.4 s, respectively. We observe a very good agreement of the three sets of results, with the low-order FEM-IE solution taking as many as 72,732 unknowns [11] (note that [11] also provides a FEM-IE solution with 12,792 unknowns, whose agreement with the MoM results is slightly worse than the one observed in Fig. 4).

As an example of metallic structures, we analyze a cubical metallic (PEC) scatterer $a = 1$ m on a side. For the purpose of the FEM-MoM analysis, the cube is symmetrically encased in an air cubical box of side length $b = 1.04$ m, as depicted in the left inset of Fig. 5. The results for the normalized monostatic RCS of the cube in a range of frequencies in Fig. 5 obtained by the FEM-MoM using a model of the first geometrical order, with the air layer around the cube represented by 6 FEM "cushions" in the form of pyramidal frusta, onto which 6 MoM square patches are attached (the mesh is shown in the right inset of the figure), are compared to experimental results [27]. The field approximation orders in the FEM elements are adopted to be 2 in the directions perpendicular to the cube faces, and 3 in other directions, whereas all current approximation orders on MoM patches are set to be 4, so that the numbers of unknowns in the hybrid solution are 328 and 384 in the FEM and MoM regions, respectively. The memory requirements are 9 MB, and computation times for filling and solving the matrices 2.2 s and 240 s, respectively, for 70 frequency points. Note the simplicity of the higher order mesh in this example, as each "cushion" between the PEC surface and FEM-MoM boundary is meshed as a single p-refined hexahedral element (entire-domain approximation). An excellent agreement of the numerical RCS results with experiment is observed, with the outer faces of the FEM hexahedra (which are the same as MoM patches) in the model being as large as about $1.8\lambda_0$ on a side (with the polynomial field/current approximation order 3 or 4) at the highest frequency considered.

As the first antenna example, consider a wire dipole antenna in the vicinity of a dielectric cube ($a = 1$ m, $\varepsilon_r = 2$). The length of the dipole equals a, and wire diameter is $2r = 1$ mm. The dipole is positioned centrally with respect to one of the cube faces, parallel to it, at a distance $d = 1$ cm, as shown in the inset of Fig. 6. The antenna is modeled by two MoM wire segments and a lumped voltage generator, and the FEM-MoM model B in Fig. 3 is used for the cube (FEM-MoM interface coincides with the dielectric surface), with the field and current expansion orders of 5 and 4, respectively, in all directions in all elements, which results in a total of 3630 FEM and 1547 MoM unknowns. The required memory resources amount to 198 MB, and the matrix fill and solution times are 1530 s and 5269 s, respectively, for 61 frequency points. In Fig. 6, we observe an excellent agreement of the higher order FEM-MoM results for

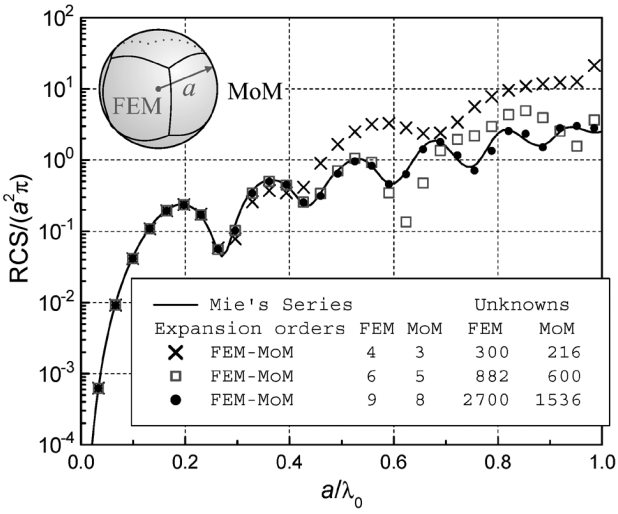

Fig. 7. Normalized monostatic radar cross section of a dielectric ($\varepsilon_{\rm r} = 2.25$) sphere: convergence analysis (taking the Mie's series solution as a reference) of the FEM-MoM method on an entire-domain (single FEM element) computational model (curved version of model A of the cube in Fig. 3) with increasing polynomial expansion orders of fields and currents (p-refinement).

the antenna input impedance with a reference pure MoM solution [25].

As an example of modeling of curved structures, Fig. 7 shows the monostatic RCS of a dielectric sphere with $\varepsilon_{\rm r} = 2.25$, normalized to the sphere cross-section area, against the normalized sphere radius a/λ_0. The results obtained by the higher order FEM-MoM are compared with the analytical solution in the form of Mie's series. The new technique is employed with a geometrical model consisting of one FEM curvilinear hexahedron and 6 MoM curvilinear patches on the surface, all of the second geometrical orders, as sketched in the figure inset, and three discretizations with increasing polynomial expansion orders of fields (FEM) and currents (MoM), as specified in the figure legend, which corresponds to a p-refinement of the solution. Note that this again represents literally an entire-domain computational model, now even a curved one (a single higher order element models a sphere), analogous to model A of the cube in Fig. 3. We observe in Fig. 7 an excellent convergence of the method with p-refinement. Additionally, when compared to the exact solution, the entire-domain model, with the coarsest mesh possible for this example, when fully p-refined (with very high orders of polynomial field and current approximations) yields an accurate RCS prediction up to the frequency at which $a/\lambda_0 = 1$ and the curved faces of the FEM hexahedron, i.e., MoM quadrilateral patches, in the model are as large as about $1.57\lambda_0$ or $2.35\lambda_{\rm diel}$ across ($\lambda_{\rm diel} = \lambda_0/\sqrt{\varepsilon_{\rm r}}$). Note that the central dimension of the hexahedron is $2\lambda_0 = 3\lambda_{\rm diel}$ (sphere diameter) at this frequency.

The last example is a helical dipole antenna near an inhomogeneous dielectric sphere, at $f = 900$ MHz. The antenna consists of a right-handed helix connected to a left-handed one (its mirror image) at the feeding point, which resides on the helix axis. Each helix has 4 full turns, of diameter $2a = 5$ mm, and a short elliptical arc providing smooth transition from the beginning of the first turn to the lumped generator at the feeding point, as shown in Fig. 8. The pitch (separation between adjacent turns) is $p = 1.25$ mm, axial height of the elliptical arc is

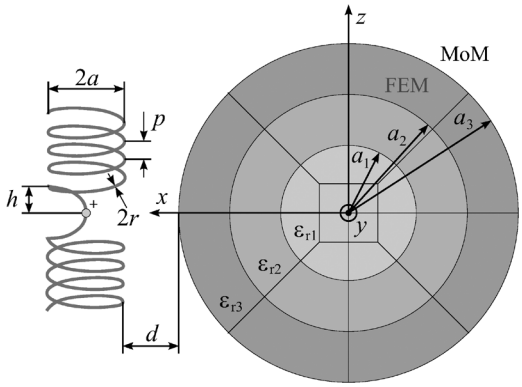

Fig. 8. Helical dipole antenna near an inhomogeneous, three-layer, dielectric sphere (picture not drawn to scale). The FEM-MoM model of the sphere, as can be seen in a cross section, consists of 8 cubical and 72 curvilinear hexahedral FEM elements of the second geometrical order, with 24 attached curvilinear quadrilateral MoM patches of the second geometrical order on the outer boundary.

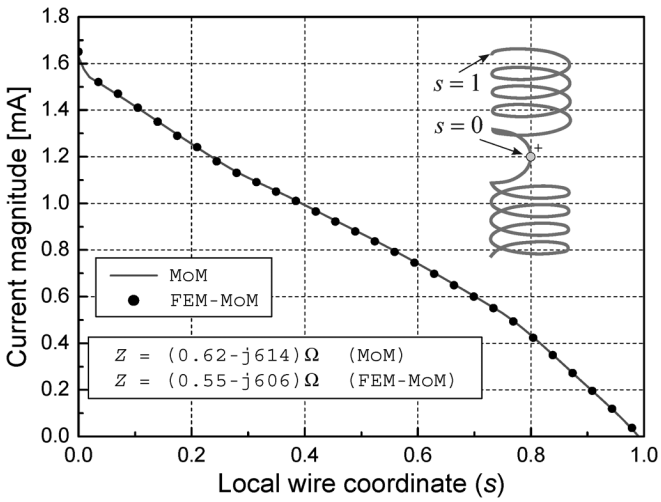

Fig. 9. Current distribution (for 1 V excitation) for the upper half of the antenna in Fig. 8, along with the antenna input impedance: comparison of a higher order FEM-MoM solution (based on the model of the sphere shown in Fig. 8) with reference pure MoM results.

$h = 1.77$ mm, wire diameter is $2r = 0.2$ mm, and distance of the helix periphery from the sphere surface is $d = 5$ mm. The sphere is composed of three concentric dielectric layers defined by radii $a_1 = 4$ cm, $a_2 = 7$ cm, and $a_3 = 10$ cm, with relative permittivities $\varepsilon_{\rm r1} = 2$, $\varepsilon_{\rm r2} = 4$, and $\varepsilon_{\rm r3} = 6$, respectively. The helical dipole is modeled by straight MoM wire segments (each helical turn is modeled by 8 equal segments and each elliptical arc by 4 equal segments), with the second-order polynomial current expansion along each of the segments. The sphere is modeled by 8 cubical and 72 curvilinear hexahedral elements of the second geometrical order in the FEM domain, along with 24 attached curvilinear quadrilateral patches of the second geometrical order in the MoM domain, as can be seen in a cross section of the model in Fig. 8. The orders of the polynomial field expansion are varied from 2 to 4 for different FEM elements and in different directions, and the orders of the polynomial current approximation for MoM patches equal 3 in all directions for all elements, with the total count of 6440 FEM and 1007 MoM unknowns (including the antenna). The required memory turns out to be 509 MB, and computation times for filling the matrices and

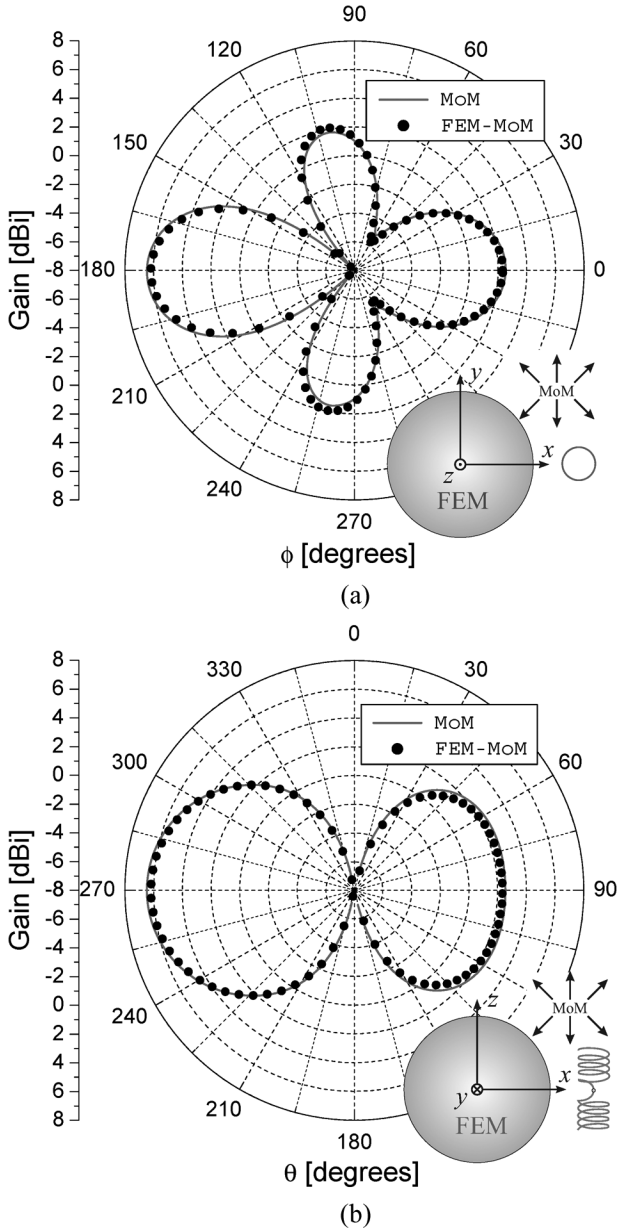

Fig. 10. Radiation patterns in the $\theta = 90^\circ$ plane (a) and $\phi = 0^\circ$ plane (b) of the antenna in Fig. 8, obtained using the higher order FEM-MoM model shown in Fig. 8 and reference pure MoM.

their solution are 518 s and 57 s, respectively. Shown in Fig. 9 is the simulated current distribution along the wire of the upper helix (for the generator voltage of 1 V), as well as the simulation result for the antenna impedance, and in Fig. 10 far field (gain) patterns in two characteristic planes of the antenna, where we see how the layered dielectric sphere enhances the system radiation toward the side at which it is placed. The results obtained by the higher order FEM-MoM are compared with the results obtained by the reference pure MoM technique [25]. We observe an excellent agreement of the two sets of results, for the current distribution, input impedance, and radiation patterns of the antenna.

IV. Conclusion

This paper has proposed a novel higher order large-domain hybrid FEM-MoM technique for modeling of radiating and scattering structures. The geometry of the structure is modeled using generalized curved parametric hexahedral and quadrilateral elements of arbitrary geometrical orders. The fields and currents on elements are modeled using curl- and divergence-conforming hierarchical polynomial vector basis functions of arbitrary approximation orders, and the Galerkin method is used for testing. As multiple MoM objects and FEM sub-regions are possible in a global generally unbounded MoM domain, the MoM part provides much greater modeling versatility and potential for applications than just as a BI closure to the FEM part. The validity, accuracy, convergence, and efficiency of the new technique have been demonstrated in several characteristic examples. The flexibility of the technique has allowed for very effective large-domain meshes that consist of a very small number of large FEM and MoM elements (e.g., a dielectric spherical scatterer analyzed using an entire-domain model with a single curved FEM element and 6 attached MoM patches on its sides), with field and current distributions of high approximation orders. All the examples have shown excellent properties of the hybrid technique and higher order elements in the context of the p-refinement of solutions, for models with both flat and curved surfaces, made from both perfectly conducting and penetrable dielectric materials, and for both scatterers and antennas. The reduction in the number of unknowns is by two orders of magnitude when compared to available data for low-order FE-BI modeling. The new hybrid FEM-MoM technique has proved to be a quite unique and useful 3-D electromagnetic computational tool for antenna and scattering problems, with an excellent potential for p-refinement procedures, especially for smooth regions, where large elements are possible.

References

[1] P. P. Silvester and R. L. Ferrari, *Finite Elements for Electrical Engineers*, 3rd ed. Cambridge, U.K.: Cambridge Univ. Press, 1996.

[2] J. M. Jin, *The Finite Element Method in Electromagnetics*, 2nd ed. New York: Wiley, 2002.

[3] J. L. Volakis, A. Chatterjee, and L. C. Kempel, *Finite Element Method for Electromagnetics*. New York: IEEE Press, 1998.

[4] *Fast and Efficient Algorithms in Computational Electromagnetics*, W. C. Chew, J. M. Jin, E. Michielssen, and J. M. Song, Eds. Norwood, MA: Artech House, 2001.

[5] J. L. Volakis, K. Sertel, and B. C. Usner, *Frequency Domain Hybrid Finite Element Methods in Electromagnetics*. London, U.K.: Morgan & Claypool , 2006.

[6] X. Yuan, D. R. Lynch, and J. W. Strohbehn, "Coupling of finite element and moment methods for electromagnetic scattering from inhomogeneous objects," *IEEE Trans. Antennas Propag.*, vol. 38, pp. 386–393, Mar. 1990.

[7] X. Yuan, "Three-dimensional electromagnetic scattering from inhomogeneous objects by the hybrid moment and finite element method," *IEEE Trans. Microw. Theory Tech.*, vol. 38, pp. 1053–1058, Aug. 1990.

[8] J.-M. Jin, J. L. Volakis, and J. D. Collins, "A finite-element-boundary-integral method for scattering and radiation by two- and three-dimensional structures," *IEEE Antennas Propag. Mag.*, vol. 33, pp. 22–32, Mar. 1991.

[9] X.-Q. Sheng, J.-M. Jin, J. Song, C.-C. Lu, and W. C. Chew, "On the formulation of hybrid finite-element and boundary-integral methods for 3-D scattering," *IEEE Trans. Antennas Propag.*, vol. 46, pp. 303–311, Mar. 1998.

[10] D. J. Hoppe, L. W. Epp, and J.-F. Lee, "A hybrid symmetric FEM/MOM formulation applied to scattering by inhomogeneous bodies of revolution," *IEEE Trans. Antennas Propag.*, vol. 42, pp. 798–805, Jun. 1994.

[11] M. N. Vouvakis, S.-C. Lee, K. Zhao, and J.-F. Lee, "A symmetric FEM-IE formulation with a single-level IE-QR algorithm for solving electromagnetic radiation and scattering problems," *IEEE Trans. Antennas Propag.*, vol. 52, pp. 3060–3070, Nov. 2004.

[12] J. Liu and J.-M. Jin, "A novel hybridization of higher order finite element and boundary integral methods for electromagnetic scattering and radiation problems," *IEEE Trans. Antennas Propag.*, vol. 49, pp. 1794–1806, Dec. 2001.
[13] J. Liu and J.-M. Jin, "A highly effective preconditioner for solving the finite element-boundary integral matrix equation of 3-D scattering," *IEEE Trans. Antennas Propag.*, vol. 50, pp. 1212–1221, Sep. 2002.
[14] M. M. Botha and J.-M. Jin, "On the variational formulation of hybrid finite element-boundary integral techniques for electromagnetic analysis," *IEEE Trans. Antennas Propag.*, vol. 52, pp. 3037–3047, Nov. 2004.
[15] Y. Ji, H. Wang, and T. H. Hubing, "A numerical investigation of interior resonances in the hybrid FEM/MoM method," *IEEE Trans. Antennas Propag.*, vol. 51, pp. 347–349, Feb. 2003.
[16] D. Jiao, A. A. Ergin, B. Shanker, E. Michielssen, and J. M. Jin, "A fast higher-order time-domain finite element-boundary integral method for 3-D electromagnetic scattering analysis," *IEEE Trans. Antennas Propag.*, vol. 50, pp. 1192–1202, Sep. 2002.
[17] C. A. Macon, L. C. Kempel, S. W. Schneider, and K. D. Trott, "Modeling conformal antennas on metallic prolate spheroid surfaces using a hybrid finite element method," *IEEE Trans. Antennas Propag.*, vol. 52, pp. 750–758, Mar. 2004.
[18] J. M. Jin, Z. Lou, Y. J. Li, N. W. Riley, and D. J. Riley, "Finite element analysis of complex antennas and arrays," *Special Issue on Large and Multiscale Computat. Electromagn., IEEE Trans. Antennas Propag.*, vol. 56, no. 8, pt. I, pp. 2222–2240, Aug. 2008.
[19] B. M. Notaroš, "Higher order frequency-domain computational electromagnetics," *Special Issue on Large and Multiscale Computat. Electromagn., IEEE Trans. Antennas Propag.*, vol. 56, no. 8, pt. I, pp. 2251–2276, Aug. 2008.
[20] J. Liu and J. M. Jin, "A special higher order finite-element method for scattering by deep cavities," *IEEE Trans. Antennas Propag.*, vol. 48, pp. 694–703, May 2000.
[21] J. M. Jin, J. Liu, Z. Lou, and C. S. T. Liang, "A fully high-order finite-element simulation of scattering by deep cavities," *IEEE Trans. Antennas Propag.*, vol. 51, pp. 2420–2429, Sep. 2003.
[22] E. A. Dunn, J.-K. Byun, E. D. Branch, and J.-M. Jin, "Numerical simulation of BOR scattering and radiation using a higher order FEM," *IEEE Trans. Antennas Propag.*, vol. 54, pp. 945–952, Mar. 2006.
[23] M. M. Ilić and B. M. Notaroš, "Higher order hierarchical curved hexahedral vector finite elements for electromagnetic modeling," *IEEE Trans. Microw. Theory Tech.*, vol. 51, no. 3, pp. 1026–1033, Mar. 2003.
[24] M. M. Ilić, A. Ž. Ilić, and B. M. Notaroš, "Higher order large-domain FEM modeling of 3-D multiport waveguide structures with arbitrary discontinuities," *IEEE Trans. Microw. Theory Tech.*, vol. 52, no. 6, pp. 1608–1614, June 2004.
[25] M. Djordjević and B. M. Notaroš, "Double higher order method of moments for surface integral equation modeling of metallic and dielectric antennas and scatterers," *IEEE Trans. Antennas Propag.*, vol. 52, no. 8, pp. 2118–2129, Aug. 2004.
[26] M. M. Ilić and B. M. Notaroš, "Higher order large-domain hierarchical FEM technique for electromagnetic modeling using Legendre basis functions on generalized hexahedra," *Electromagnetics*, vol. 26, pp. 517–529, Oct. 2006.
[27] A. Yaghjian and R. McGahan, "Broadside radar cross section of the perfectly conducting cube," *IEEE Trans. Antennas Propag.*, vol. 33, pp. 321–329, Mar. 1985.

Milan M. Ilić (S'00–M'04) was born in Belgrade, Serbia, in 1970. He received the Dipl. Ing. and M.S. degrees in electrical engineering from the University of Belgrade, in 1995 and 2000, respectively, and the Ph.D. degree from the University of Massachusetts Dartmouth, in 2003.

From 1995 to 2000, he was a Research and Teaching Assistant in the School of Electrical Engineering, University of Belgrade. From 2000 to 2003, he was a Ph.D. student and a Research Assistant at the University of Massachusetts Dartmouth, where he continued to work as a Postdoctoral Research Associate during 2003 and 2004. He is currently an Assistant Professor in the School of Electrical Engineering at the University of Belgrade and a postdoctoral Research Associate with the ECE Department, Colorado State University, Fort Collins. His research interests include computational electromagnetics, antennas, and microwave components and circuits.

Dr. Ilić was the recipient of the 2005 IEEE MTT-S Microwave Prize.

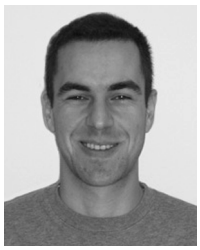

Miroslav Djordjević (S'00–M'04) was born in Ćuprija, Serbia, in 1973. He received the Dipl. Ing. degree from the University of Belgrade, Belgrade, Serbia, in 1998, the M.S. degree from the University of California, Los Angeles (UCLA), in 2000, and the Ph.D. degree from the University of Massachusetts (UMass) Dartmouth, in 2004.

From 1998 to 2000, he was a Graduate Student Researcher at Antenna, Research and Measurement (ARAM) Laboratory, UCLA. From 2000 to 2003, he was a Research Assistant at UMass Dartmouth, where he was a Postdoctoral Associate in 2004. From 2004 to 2006 he was a Senior Engineer at Antenna Research Associates, Inc., Beltsville, MD. From 2007 to 2008, he was a Research Scientist at IMTEL Komunikacije, Belgrade, Serbia. He is currently a Professor at ICT College, Belgrade, Serbia. His research interests are in higher order modeling, hybrid methods, and analysis and design of ultra wide-band and vehicle mounted antennas.

Andjelija Ž. Ilić (S'01–M'04) was born in Belgrade, Serbia, in 1973. She received the Dipl. Ing. degree in electrical engineering from the University of Belgrade, in 1998 and the M.S. degree from the University of Massachusetts Dartmouth, in 2004.

From 1999 to 2001, she was a Research and Teaching Assistant in the School of Electrical Engineering, University of Belgrade, Serbia. From 2002 to 2004, she was a student in the M.S. program and a Research Assistant at the University of Massachusetts Dartmouth. She is currently with the Vinca Institute of Nuclear Sciences, Belgrade, and a Ph.D. student with the School of Electrical Engineering at the University of Belgrade. Her research interests include mathematical modeling, computational and applied electromagnetics, and particle beam dynamics.

Branislav M. Notaroš (M'00–SM'03) was born in Zrenjanin, Yugoslavia, in 1965. He received the Dipl.Ing. (B.Sc.), M.Sc., and Ph.D. degrees in electrical engineering from the University of Belgrade, Belgrade, Yugoslavia, in 1988, 1992, and 1995, respectively.

From 1996 to 1998, he was an Assistant Professor in the Department of Electrical Engineering at the University of Belgrade. He spent the 1998–1999 academic year as a Research Associate at the University of Colorado at Boulder. He was an Assistant Professor, from 1999 to 2004, and Associate Professor, from 2004 to 2006, in the Department of Electrical and Computer Engineering at the University of Massachusetts Dartmouth. He is currently an Associate Professor of electrical and computer engineering at Colorado State University, Fort Collins. His research and teaching interests and activities are in theoretical and computational electromagnetics and in antennas and microwaves. His publications include about 70 journal and conference papers, and five textbooks and workbooks.

Dr. Notaroš was the recipient of the 2005 IEEE MTT-S Microwave Prize, 1999 IEE Marconi Premium, and 2005 UMass Dartmouth Scholar of the Year Award.